Available online at www.sciencedirect.com

jmr&t
Journal of Materials Research and Technology

journal homepage: www.elsevier.com/locate/jmrt

Original Article

Rutile TiO2 thin films growth on glass substrates with generation of high entropy interface

M.E.P. Missner [a], J. Stryhalski [b], M. Tomiyama [c], P. Soares [d], A.A.C. Recco [c], L.C. Fontana [c,*]

[a] Textile Engineering Department, Santa Catarina Federal University – UFSC Blumenau, Santa Catarina, 89036-002, Brazil
[b] Santa Catarina Federal Institute - IFSC Jaraguá Do Sul, Santa Catarina, 89254-430, Brazil
[c] Laboratory of Plasmas, Films and Surfaces Center for Technological Sciences, UDESC, Joinville, Santa Catarina, 89.219-710, Brazil
[d] Mechanical Engineering Department, Polytechnic School, Pontifical Catholic University of Parana- PUCPR Curitiba, Paraná, 80215901, Brazil

ARTICLE INFO

Article history:
Received 8 February 2023
Accepted 9 March 2023
Available online 14 March 2023

Keywords:
Thin film Rutile TiO2
Sputtering
Hydrophilic
High entropy interface

ABSTRACT

TiO_2 thin films obtained through Reactive Magnetron Sputtering (RMS) have been extensively studied in the last decades for several applications as photocatalyst and self-cleaning coats. However, reactive deposition through MS onto large area substrates can be troublesome due to inhomogeneous films thickness and poor adhesion between film and substrate. This paper investigates the deposition of TiO_2 thin films on glass substrates through a two steps method, namely: 1- deposition of nanometer thickness Ti metallic films on glass substrate, through triode magnetron sputtering; 2- oxidation of the Ti film through thermal treatment in atmospheric air, to obtain stoichiometric TiO_2 layers. The film oxidation was performed concomitantly to the glass thermal treatment carried out at 650 °C. Analysis through XPS depth profile indicates the formation of a chemically graded high entropy interlayer due to the interdiffusion of atoms from substrate to film and vice-versa, during the thermal treatment. The high entropy interface layer contributes to reduces the mismatch between the film and the substrate lattice, resulting in an improvement of film adhesion. The badgap analysis through Tauc method show two energy values, namely 3.2 eV and 2.9 eV, which can be attributed to TiO_2-rutile layer and the high entropy zone at interface, composed by $[Ca\text{-}Na\text{-}Si\text{-}Ti]O_x$ oxides. The wettability results show that the contact angle may be as low as 10° between a deionized water drop and the rutile-TiO_2 surface, after activation with UV light irradiation, which is characteristic of super-hydrophilic surface.

© 2023 The Author(s). Published by Elsevier B.V. This is an open access article under the CC BY-NC-ND license (http://creativecommons.org/licenses/by-nc-nd/4.0/).

* Corresponding author.
E-mail address: luis.fontana@udesc.br (L.C. Fontana).
https://doi.org/10.1016/j.jmrt.2023.03.072
2238-7854/© 2023 The Author(s). Published by Elsevier B.V. This is an open access article under the CC BY-NC-ND license (http://creativecommons.org/licenses/by-nc-nd/4.0/).

1. Introduction

Titanium dioxide (TiO_2) is a well-known semiconductor material, which has promising chemical and physical properties such as high refractive index, photoinduced hydrophilicity, wide band gap, high physical and chemical stability, while being a nontoxic material [1–8]. TiO_2 thin films have been used in a wide application range, as photocatalyst, gas sensing element, optical coatings, in water and air purification applications, corrosion barrier, in solar cells in electrical devices such as varistors and self-cleaning surfaces [9–12]. Another interesting point is the inactivation of bacteria and virus provided by TiO_2 photocatalysis effects, under UV light irradiation [13].

Solar UV-radiation can induce simultaneously catalytic and hydrophilic characteristics on the same surface of TiO_2 films, through different mechanisms. Both, hydrophilicity and photocatalysis, can contribute to the "self-cleaning" property of glass surfaces which may prevent the harm caused by dust and pollutants [14–17]. The TiO_2 photocatalytic properties are due to charge carriers (hole and electron) generated through ultraviolet (UV) radiation on TiO_2 surface. The photogenerated holes can oxidize nearby organic molecules on the TiO_2 surface. In addition, electrons in the conduction band may participate in reduction processes, which typically react with molecular oxygen in the air to produce superoxide radical anions [9–14]. The superhydrophilicity is due to chemical changes on surface. The photogenerated holes may react with adsorbed water molecules, forming singly coordinated OH groups which have high surface energy and, consequently, generating a superhydrophilic surface [18–22]. Self-cleaning TiO_2 transparent films on solar cells may prevent power losses up to 25% caused by dust pollution, which may significantly degrade the efficiency of outdoor-installed solar modules [23,24]. Surface modification of building materials such as glass windows and facades with transparent TiO_2 thin films helps keeping the building's exterior clean by utilizing UV solar radiation [25–29].

Different techniques have been used for TiO_2 film deposition, such as sol–gel processing, spray pyrolysis and reactive magnetron sputtering [30,31]. The sol–gel processing is accepted as an economical and promising technique for generating nanocrystalline TiO_2 coatings on different substrates, including glass surface [32]. One of the most studied techniques is the spray pyrolysis, due to its simplicity and cost-effectiveness for mass production [33]. The methods providing the most dense and porous-free films are the Magnetron Sputtering processes, such as the DC Sputtering, HiPIMS or RF Sputtering. However, the TiO_2 film deposition reactive-mode Magnetron Sputtering, on large-area glass substrates, can yield high internal stress and poor crystallinity, which may adversely affect the film adhesion and photocatalytic properties [34].

Considering the drawbacks associated to TiO_2 film deposition on glass substrates using Reactive Magnetron Sputtering, the present paper aims to prepare such films in two steps: 1- deposition of nanometric thickness Ti metallic film on glass substrates through Triode Magnetron Sputtering (TMS) and 2- oxidation of Ti films by heat treatment in atmospheric air, with thermodynamic parameters similar to those used in the glass-toughening process. Deposition of Ti metallic films through Triode Magnetron Sputtering, provides dense films with good adhesion to substrate and easy layer thickness control. It allows the deposition of nanometric-thick films on large-area glass substrates. On the other hand, the oxidation of the metallic Ti films can take place simultaneously to the glass quenching process, producing transparent, photocatalytic and self-cleaning TiO_2 films. The diffusion of atoms through interface, from substrate to film and vice-versa, may improve the film adhesion due to the formation of ahigh-entropy alloy zone at interface. Indeed, investigations through XPS measurements have shown that, at interface layer, comes up a high-entropy alloy zone composed by atoms from substrate and atoms from the film. However, atoms from substrate don't reach the top of the film, which keep the surface as pure TiO_2, and so, its properties are preserved.

2. Experimental details

The metallic Ti film deposition was performed using a pulsed DC triode magnetron sputtering system (TMS) [35]. The sputtering from a Ti target (99.5% purity) was performed for 3.0 min in Argon atmosphere. The argon plasma was generated through a DC pulsed power supply (Pinnacle Plus 5 kW). Table 1 shows the parameters used for the film deposition, which were based on a previous study [36,37].

The deposition chamber is a stainless-steel cylindrical volume, with a diameter of 280 mm and a height of 240 mm. The magnetron was water-cooled and the vacuum was produced through a turbo molecular pump system. The soda-lime glass substrates were 30 × 10 × 4 mm^3 rectangular samples.

The depositions were carried out on samples heated to 300 °C using a resistive heater. The chamber pressure was pumped down to the base pressure of 10^{-5} Torr (1.3×10^{-3} Pa). The work pressure, during the film depositions, was kept at 3.0×10^{-3} Torr (0.4 Pa).

The samples were named according to the heat treatments performed after de deposition, as shown in Table 2.

Table 1 – Parameters used in the present paper for metallic Ti film deposition through Magnetron Sputtering.

Parameters		Value
Argon flow (sccm)		2.8
Base pressure in the chamber (Pa)		1.3×10^{-3}
Working pressure (Pa)		0.4
Film deposition time (min)		3.0
Substrate temperature (°C)		300
Bias	Power (W)	470
Cathode (target Ti)	Frequency (kHz)	20.0
	Time on - T_{on} (μs)	48
	Duty Cycle (%)	96
Bias	Voltage (V)	−100
Substrate	Frequency (kHz)	150
	Time on - T_{on} (μs)	2.6
	Duty Cycle (%)	40

Table 2 – Samples names according to the treatments performed.

	Without oxidation	Oxidation at 500 °C	Oxidation at 650 °C
Sample	WO	O500	O650

One set of samples of Ti films was oxidized at 500 °C, and another set of Ti films was oxidized at 650 °C, during 1 h. The heating rate was 20 °C/min and the cooling rate was 10.3 °C/min, as shown in Fig. 1.

The thin TiO_2 films were characterized through the following techniques: Grazing Incidence X-ray diffraction (GIXD), spectrophotometry (transmittance, reflectance and *band gap* energy measurement through Tauc plot analysis), surface topography and roughness through AFM analysis, thickness measurement, X-ray photoelectron spectroscopy (XPS) and wettability through contact angle of water drop (sessile drop method).

Grazing Incidence X-ray Diffraction (GIXD) analysis, with a grazing incidence angle of 1°, was performed with a XRD-7000 Shimadzu equipment, Cu k_α = 1.5406 Å radiation with a scanning speed of 2°/min, current of 30 mA and voltage of 40 kV. Optical measurements of transmittance and reflectance were made in the wavelength range 200 ≤ λ ≤ 1200 nm using a UV-3600 Plus Shimadzu spectrophotometer. Film roughness was determined from images obtained with a Nanosurf Nanite Atomic Force Microscope (AFM), operating in static mode, with a 20 nm Si tip. The images were standardized with an area of 5 × 5 μm and the "z" axis at 75 nm.

The contact angle measurements (ramé-hart 590) were performed before and after the sample exposure to UVC irradiation (λ = 254 nm) for 24 h in a UV cabinet box (11W). After the UV irradiation, the contact angle measurements were performed for the following times: 0 h, 24 h and 48 h [36–38]. Between the consecutive contact angle measurements, the samples were kept in a dark box. The volume of the water drop used to measure the contact angle was 5.0 μl. The film chemical composition depth profile, from the surface to the film/substrate interface, was measured though XPS technique (Thermo Scientific k-alfa), with an analyzer mode pass energy of 200.0 eV and a spot size of 30 μm. Film thickness was measured through stylus profilometry (Dektak xt) on a relief molded by placing a small mask on the sample surface, during the Ti film deposition.

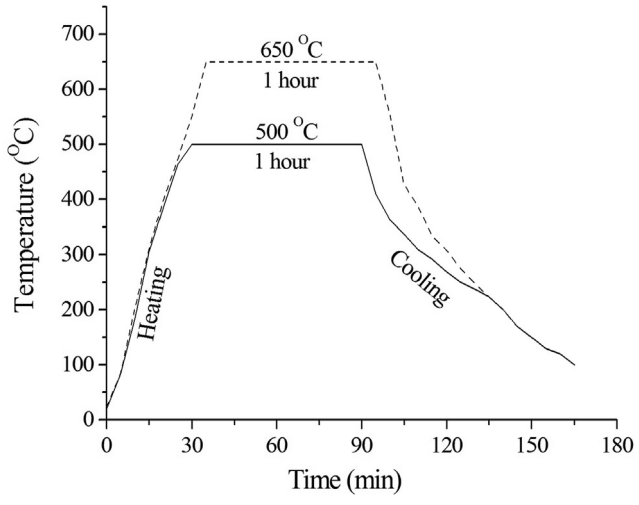


Fig. 1 – Heating and cooling ramp used for oxidation of Ti films on glass substrate.

3. Results and discussion

Fig. 2 shows the X-ray diffraction of samples WO, O500 and O650. For samples without heat treatment (WO), the X-ray spectra show only wide peaks relative to a pure titanium structure, indicating a semicrystalline structure of the film at condition as deposited. For the samples treated at 650 °C, only peaks referring to the Rutile TiO_2 are observed, indicating the oxidation of the entire film. For the films treated at 500 °C, traces of peaks corresponding to pure titanium (Ti (202), Ti (200) and Ti (100)) were observed.

Other peaks found in samples O500 are related to the rutile phase with the following texture: (110), (101), (200), (111), (211), (220) and (002). These results suggest that the films were not oxidized throughout its entire thickness during the 500 °C heat treatment, a fact that is corroborated by the low transmittance of those samples. No Anatase peaks were observed in any of the films, indicating that those treatment conditions favor the rutile structure formation. Mohamed (2022), deposited TiO_2 films on heated substrates 300 °C and resulted in crystalline anatase phase [39].

Fig. 3 shows the optical transmittance results as a function of the incident radiation wavelength. The colorless soda-lime glass substrate presents higher transmittance in the visible range (400–780 nm). In the ultraviolet region (λ < 400 nm), the transmittance values suddenly drop for both the glass samples without films and the O650 samples, because the incident photons' energy (UV) is higher than the TiO_2 and the glass' band gap value, so the radiation do not pass through the film.

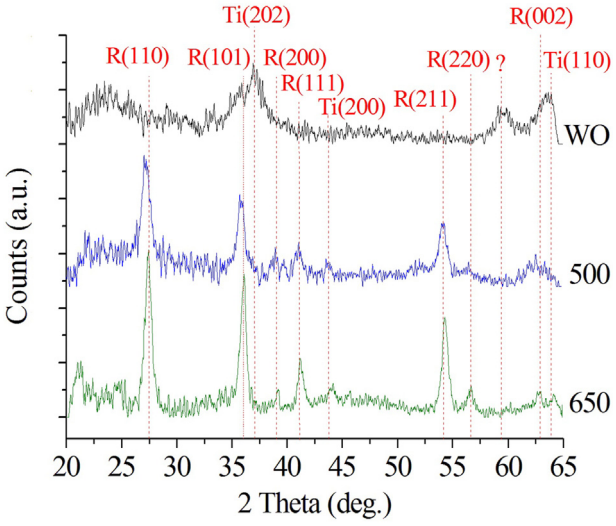


Fig. 2 – GIXRD patterns of TiO_2 films corresponding to samples WO, O500 and O650. Legend: R = Rutile; Ti = Metallic Titanium.

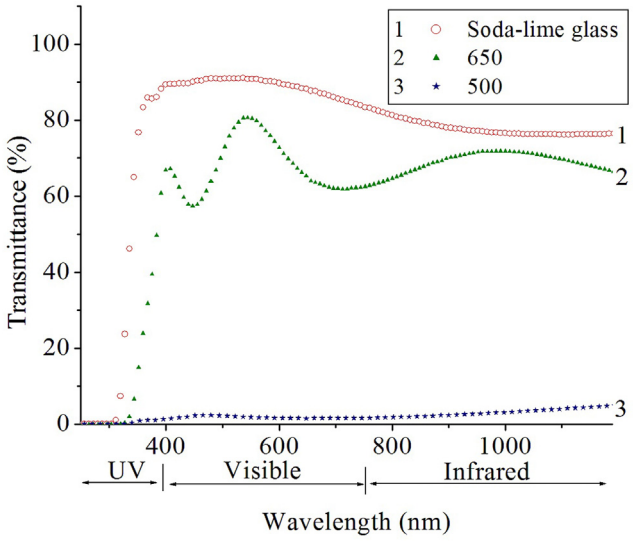


Fig. 3 – Optical transmittance spectra for the following samples of soda-lime glass: (1) without film; (2) O650 sample; (3) O500 sample.

The absorption of radiation by electrons, which jump from the valence band to the conduction band, activates the TiO_2 surface. On the other side, within the wavelength range above 700 nm (i.e. the infrared range), the transmittance is typical of the glass material: the incident radiation causes vibration only in the crystalline lattice and little transmittance attenuation [17]. For the O500 samples, the transmittance values are near zero, since the films are opaque even after oxidation, suggesting that the films were not oxidized throughout their whole thicknesses (~200 nm). This finding agrees with the XRD results (Fig. 2), in which traces of metallic Ti peaks were found. Conductive materials, e. g. metallic Ti, show negligible optical transmittance due to the absorbance of radiation by free electrons in the conduction band [40].

The band gap energy for the soda-lime glass used in the present study was obtained through the Tauc method. Its value is Eg = 3.5 eV, which corresponds to a wavelength of $\lambda = 358$ nm, located in the ultraviolet region.

In the case of the combined film/glass, absorption of radiation may take place in both the film and the glass substrate. The difference between the energy absorbed by the neat substrate and by the aggregate "film/substrate" can be attributed to film absorption. The absorption coefficient α is a function of the wavelength λ and can be determined by the following relation [41–44].

$$\alpha(\lambda) = \frac{\ln[(1-R)/T]}{d} \quad (1)$$

where T, R and d are the spectral transmittance, reflectance and film thickness, respectively.

Once the energy absorption in the film is obtained as a function of the radiation wavelength through the Tauc method (considering indirect transitions) [45], the band gap energy Eg of the TiO_2 films can be calculated through equation (2) [41,42].

$$(\alpha h\nu) = B(h\nu - E_g) \quad (2)$$

where $h\nu$ and B are the photon energy and the absorption constant, respectively (B is independent of ν). The band gap energy is obtained as the interception of the curve $(\alpha h\nu)^{1/2}$ versus $h\nu$ in the high absorbance region. For the soda-lime glass substrate used in this paper, the band gap values were Eg = 3.5 eV. Fig. 4 shows the Tauc plot for indirect transition [46], in the TiO_2 range of absorption, where a double gap is observed with values of 2.9 eV and 3.2 eV for the O650 sample. We propose two hypotheses for the double gap, namely: (1) the film may be composed of two layers, that is, rutile and suboxides TiO_x (x>2) [47] and (2) a transient layer of TiO_2 contaminated by atoms diffused from the substrate to the film [46–49], which can produces a high-entropy alloy zone due to the heat treatment.

It is well known that the Eg values for annealed TiO_2 are 3.0 eV and 3.2 eV for the rutile and the anatase phases, respectively [50–52]. Those values can change if the film is not stoichiometric (for examples suboxides), if the film contains residual internal stress or, in addition, if the film is contaminated with other chemical elements [43,44]. The double gap observed in Fig. 4 cannot be attributed to a film composed of anatase and rutile, because the GIXD results only show the rutile. Another hypothesis is the formation of a high-entropy alloy zone at interface, due to the atomic interdiffusion between the film and the substrate. Fig. 5 shows XPS depth profile results for the O650 sample, which reveal atoms of Si, Na and Ca in the film.

Atoms diffused from the substrate can reach approximately half of the film thickness and this fact corroborates the hypothesis that the additional gap is due to the contamination of the TiO_2 with atoms from the substrate, which produces a high-entropy alloy zone composed by $[Si\text{-}Na\text{-}Ca\text{-}ti]O_x$. It is

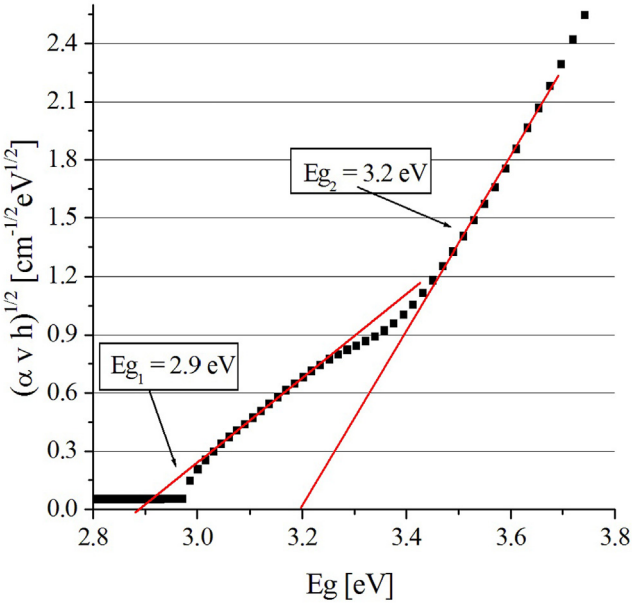


Fig. 4 – Band Gap energy plot using the Tauc method. A double gap can be observed for samples treated at 650 °C, namely $E_{g1} = 2.9$ eV and $E_{g2} = 3.2$ eV.

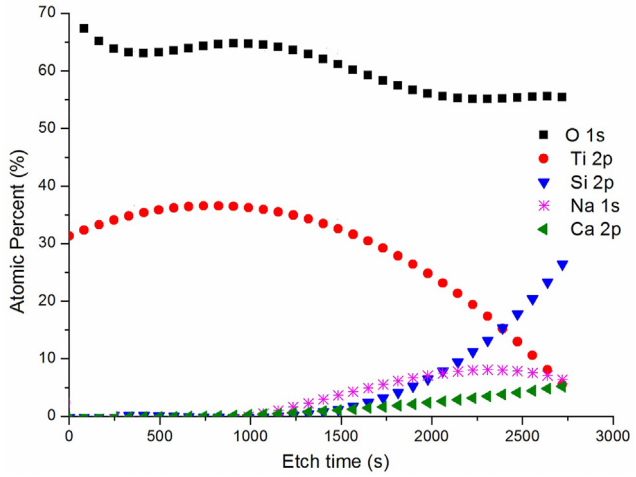


Fig. 5 – XPS measurements showing the film's depth composition profile, indicating that there is diffusion of atoms from the substrate (Si, Na, Ca) into the TiO_2 film.

important point that the high-entropy alloy zone may improve the adhesion through matching better the structure of film and substrate. On the other hand, the proportion of oxygen and titanium near the film surface correspond to stoichiometric TiO_2. The maintenance of titanium dioxide at surface is crucial to preserve the well known optical and catalytic properties of TiO_2.

Fig. 6 shows images obtained through atomic force microscopy (AFM) technique, with an area of 5 μm × 5 μm and a "z" axis height of 150 nm.

Roughness is observed to increase after the sample's oxidation treatment. In addition, film roughness oxidized at 650 °C is significantly greater than that of the film oxidized at 500 °C. Film oxidation demands recrystallization and volumetric increase, which result in further roughness. The oxide tends to expand laterally, but it suffers substrate constraints, which produces compressive stress at the film (in the plane of the oxide layer) and a reciprocal tensile stress on the substrate. So, the bond between layer/substrate need be sufficiently strong to support the stress and do not suffer spalling and de-cohesion at interface. On the other hand, B. Panicaud et al. (2006) [53] shown that the grains can suffer a creep perpendicular to the interfaces, which produces stress relaxation and increasing of film thickness. Results of film thickness increasing, observed in present paper, are show in Table 3. The volume of the Ti unit cell (metal Ti-hcp) is $105.6 \times 10^{-30}\ m^3$, which contains two Ti atoms in the cell. After Ti film oxidation through thermal treatment, the rutile crystalline structure (tetragonal) was obtained, whose unit cell has volume of $62.4 \times 10^{-30}\ m^3$, which contains six Ti atoms[2]. Thereby, the Ti atomic density ratio between those structures is 1.8. Consequently, if the film were totally oxidized, its thickness would increase by a factor close to 1.8. Table 3 shows that the film treated at 500 °C was not completely oxidized, since the ratio $e_{500}/e_{WO} = 1.4 \pm 0.2$ is less than the 1.8 factor, which is in accordance with the results of low film transmittance in sample O500 (Fig. 3). For the film treated at 650 °C, the thickness ratio is $e_{650}/e_{WO} = 1.9 \pm 0.2$ (close to 1.8),

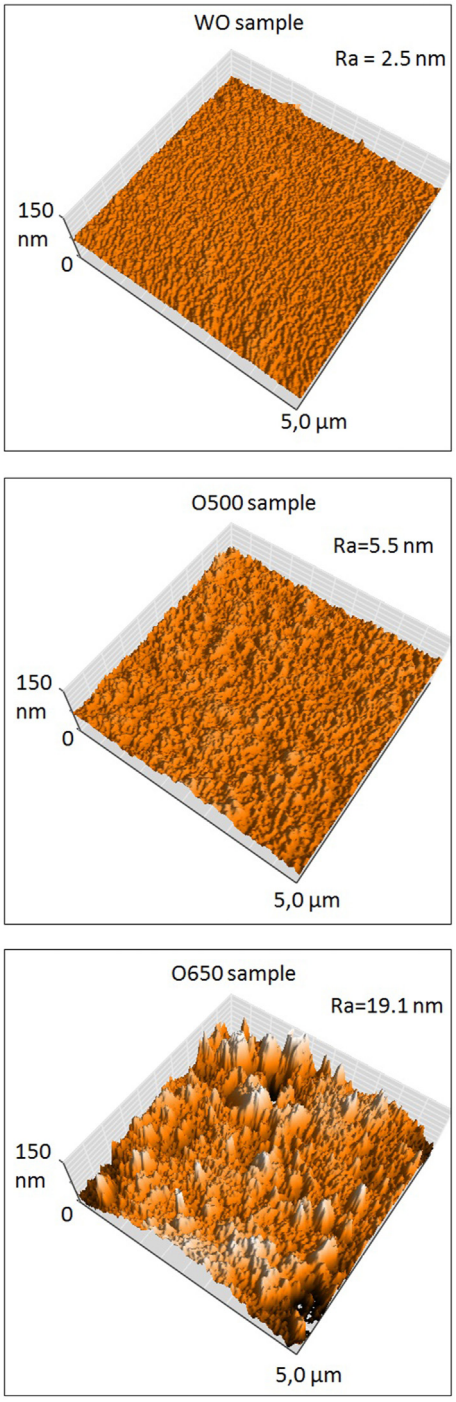


Fig. 6 – Topography and nanoscale roughness R_a obtained through AFM analysis: a) WO, b) O500 and c) O650 samples.

which indicates that the film was completely oxidized, which is corroborated by the high transmittance found for those films. In addition, it is important to point that there was not observed any signal of film spalling and de-cohesion, which indicates that the high-entropy alloy zone at interface, composed by $[Si\text{-}Na\text{-}Ca\text{-}ti]O_x$ produces a strong adhesion film/substrate.

Fig. 7 shows the contact angle measurements for samples WO, O500 and O650, carried out before and after the film

Table 3 – Film thickness (nm) before and after treatment at 500 °C and 650 °C.

	WO	O500	O650
Film thickness (nm)	130	190	260
Thickness increase Ratio	1.00	1.40 ± 0.20	1.90 ± 0.20

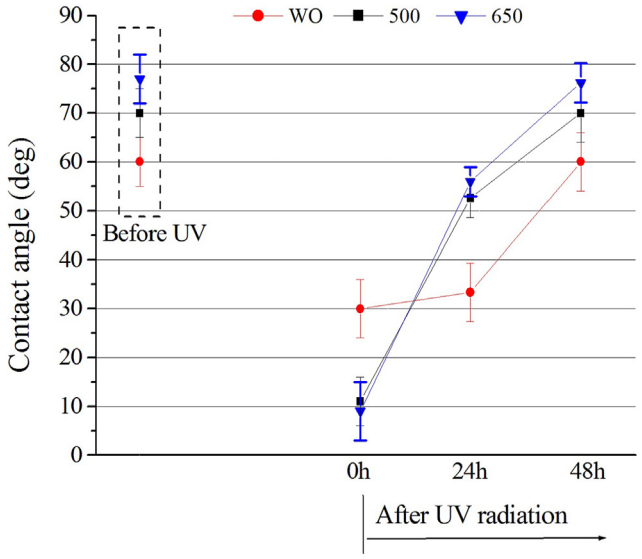


Fig. 7 – Contact angle measurements: before UVC irradiation and after UVC irradiation (λ = 254 nm) during 24 h in a UV cabinet box.

irradiation with UVC light. Before the UVC irradiation, the samples showed contact angles between 60° and 80°.

After the irradiation, the contact angle for the O500 and the O650 samples were observed to go down to 10°, becoming a super-hydrophilic surface. After a 48-h aging (from the UV irradiation), the contact angle returned to the original values, those from before the UVC irradiation. For the WO samples, the contact angle was observed to decrease to 30° after the UV irradiation. Although the WO samples did not undergo a thermal oxidation treatment, there is a very thin surface oxide layer (TiO_2) that naturally forms under ambient conditions. That natural layer can also be activated by UVC, which results in a decrease in the contact angle.

The UVC irradiation on TiO_2 films can increase the surface energy and, consequently, improve the hydrophilicity through two main mechanisms: 1- the photo-generation of a hole–electron pair on the surface and 2- the oxygen desorption from the TiO_2 structure. Due to the oxygen vacancies generated in the structure, there is a new balance of charges, where some cations Ti^{4+} are converted into Ti^{3+} on the surface. Therefore, it acts as traps for water molecules adsorption, enhancing the surface's hydrophilic characteristic [54–57]. In addition, by increasing the hydrophilicity, we improve the "self-cleaning" property of the glass surface.

4. Conclusion

Rutile TiO_2 was obtained from thermal oxidation of metallic Ti films deposited on glass substrates through grid-assisted magnetron sputtering. The thermal oxidation ($Ti + O_2 \rightarrow TiO_2$) carried out in atmospheric air at 650 °C during 1.0 h (i.e. similar parameters to those used in glass temper processes) provides an oxide growth rate that is high enough to oxidize a whole 130-nm-thick Ti film. After the oxidation, the titanium film has increased in thickness at a ratio of 1.8, approximately. Despite the considerable increase in thickness, it was not observed any evidence of spalling and de-cohesion, which indicates that the high-entropy alloy zone at interface, composed by $[Si\text{-}Na\text{-}Ca\text{-}Ti]O_x$, produces a strong adhesion film/substrate. The TiO_2 films exhibit the crystallized Rutile phase, with a transmittance of about 70% in the visible range, and two Band Gap values: 2.9 eV and 3.2 eV. The origin of the second gap may be related to the formation of an under-layer contaminated by substrate atoms. In fact, the XPS depth profile analysis showed a concentration gradient of substrate atoms (Si, Ca, Na) toward the film, from the film/substrate interface. However, those atoms do not reach the film surface, keeping it as pure Rutile TiO_2. The contact angle of a deionized water drop on the Rutile TiO_2 surface was as low as 10° (after UV irradiation). Results presented in this paper indicate that this film deposition methodology can be a good alternative for the coating of large-area substrates with TiO_2 films, which can provide the properties of photocatalysis and self-cleaning to flat glass surfaces.

Declaration of Competing Interest

The authors declare that they have no known competing financial interests or personal relationships that could have appeared to influence the work reported in this paper.

Acknowledgements

This work was partially supported by PRONEM-FAPESC-CNPq-2020TR730, Brazil, and FAPESC/UDESC/PAP 2021TR874, Brazil.

REFERENCES

[1] Pelaez M, Nolan NT, Pillai SC, Serry MK, Falaras P, Kontos AG, et al. A review on the visible light active titanium dioxide photocatalysts for environmental applications. Appl Catal B Environ 2012;125:331–49. https://doi.org/10.1016/j.apcatb.2012.05.036.

[2] Kang X, He Y, Song X, Tan Z. Titanium dioxide: from engineering to applications. Catalysts 2019;9(2):191. https://doi.org/10.3390/catal9020191.

[3] Liao C, Li Y, Chin Tjong S. Visible-light active titanium dioxide nanomaterials with bactericidal properties. Nanomaterials 2020;10(1):124. https://doi.org/10.3390/nano10010124.

[4] De Silva NL, Jayasundera AC, Folger A, Kasian O, Zhang S, Yan CF, et al. Superior solar-to-hydrogen energy conversion efficiency by visible light-driven hydrogen production via highly reduced Ti 2+/Ti 3+ states in a blue titanium dioxide photocatalyst. Catal Sci Technol 2018;8(18):4657–64. https://doi.org/10.1039/C8CY01212A.
[5] Andronic L, Lelis M, Enesca A, Karazhanov S, et al. Photocatalytic activity of defective black-titanium oxide photocatalysts towards pesticide degradation under UV/VIS irradiation. Surface Interfac 2022;32:102123.
[6] Ratova M, Klaysri R, Praserthdam P, Kelly PJ. Visible light active photocatalytic C-doped titanium dioxide films deposited via reactive pulsed DC magnetron co-sputtering: properties and photocatalytic activity. Vacuum 2018;149:214–24. https://doi.org/10.1016/j.vacuum.2018.01.003.
[7] Arora I, Chawla H, Chandra A, Sagadevan S, Garg S. Advances in the strategies for enhancing the photocatalytic activity of TiO2: conversion from UV-light active to visible-light active photocatalyst. Inorg Chem Commun 2022:109700. https://doi.org/10.1016/j.inoche.2022.109700.
[8] Barbieriková Z, Pližingrová E, Motlochová M, Bezdička P, Boháček J, Dvoranová D, et al. N-Doped titanium dioxide nanosheets: preparation, characterization and UV/visible-light activity. Appl Catal B Environ 2018;232:397–408. https://doi.org/10.1016/j.apcatb.2018.03.053.
[9] Diebold U. The surface science of titanium dioxide. Surf Sci Rep 2003;48:53–229. https://doi.org/10.1016/S0167-5729(02)00100-0.
[10] Haider AJ, Jameel ZN, Al-Hussaini IH. Review on: titanium dioxide applications. Energy Proc 2019;157:17–29. https://doi.org/10.1016/j.egypro.2018.11.159.
[11] Padmanabhan NT, John H. Titanium dioxide based self-cleaning smart surfaces: a short review. J Environ Chem Eng 2020;8(5):104211. https://doi.org/10.1016/j.jece.2020.104211.
[12] Wang B, Wei S, Guo L, Wang Y, Liang Y, Xu B, et al. Effect of deposition parameters on properties of TiO2 films deposited by reactive magnetron sputtering. Ceram Int 2017;43:10991–8. https://doi.org/10.1016/j.ceramint.2017.05.139.
[13] Nakano R, Ishiguro H, Yao Y, Kajioka J, Fujishima A, Sunada K, et al. Photocatalytic inactivation of influenza virus by titanium dioxide thin film. Photochem Photobiol Sci 2012;11(8):1293. https://doi.org/10.1039/c2pp05414k.
[14] Deubener J, Helsch G, Moiseev A, Bornhöft H. Glasses for solar energy conversion systems. J Eur Ceram Soc 2009;29:1203–10. https://doi.org/10.1016/j.jeurceramsoc.2008.08.009.
[15] Shukrullah S, Ayyaz M, Naz MY, Ibrahim KA, AbdEl-Salam NM, Mohamed HF. Post-synthesis plasma processing and activation of TiO2 photocatalyst for the removal of synthetic dyes from industrial wastewater. Appl Phys A 2021;127(5):1–10. https://doi.org/10.1007/s00339-021-04467-z.
[16] Kim DJ, Kang JY, Kim KS. Preparation of TiO2 thin films on glass beads by a rotating plasma reactor. J Ind Eng Chem 2010;16(6):997–1000. https://doi.org/10.1016/j.jiec.2010.07.005.
[17] Weng KW, Huang YP. Preparation of TiO2 thin films on glass surfaces with self-cleaning characteristics for solar concentrators. Surf Coating Technol 2013;231:201–4. https://doi.org/10.1016/j.surfcoat.2012.06.058.
[18] Nakata K, Fujishima A. TiO2 photocatalysis: design and applications. J Photochem Photobiol C Photochem Rev 2012;13:169–89. https://doi.org/10.1016/j.jphotochemrev.2012.06.001.
[19] Moma J, Baloyi J. Modified titanium dioxide for photocatalytic applications. Photocatalysts-Applications and Attributes 2019;18:10–5772. https://doi.org/10.5772/intechopen.79374.
[20] Bannier E, Darut G, Sánchez E, Denoirjean A, Bordes MC, Salvador MD, et al. Microstructure and photocatalytic activity of suspension plasma sprayed TiO2 coatings on steel and glass substrates. Surf Coating Technol 2011;206(2–3):378–86. https://doi.org/10.1016/j.surfcoat.2011.07.039.
[21] Jung CK, Bae IS, Song YH, Boo JH. Plasma surface modification of TiO2 photocatalysts for improvement of catalytic efficiency. Surf Coating Technol 2005;200(5–6):1320–4. https://doi.org/10.1016/j.surfcoat.2005.07.097.
[22] Mohammadizadeh MR, Bagheri M, Aghabagheri S, Abdi Y. Photocatalytic activity of TiO2 thin films by hydrogen DC plasma. Appl Surf Sci 2015;350:43–9. https://doi.org/10.1016/j.apsusc.2015.03.196.
[23] Weng KW, Huang YP. Preparation of TiO2 thin films on glass surfaces with self-cleaning characteristics for solar concentrators. Surf Coating Technol 2013;231:201–4. https://doi.org/10.1016/j.surfcoat.2012.06.058.
[24] Salimian J, Osfouri S, Azin R, Jalali T. Impacts of paste preparation methods on the porous TiO2 nanostructure properties and naturally dye-sensitized solar cells performance. J Mater Res Technol 2022;18:4816–33.
[25] Murugan K, Subasri R, Rao TN, Gandhi AS, Murty BS. Synthesis, characterization and demonstration of self-cleaning TiO2 coatings on glass and glazed ceramic tiles. Prog Org Coating 2013;76:1756–60. https://doi.org/10.1016/j.porgcoat.2013.05.012.
[26] Wang X, Zeng J, Yu X, Liang C, Zhang Y. Water harvesting method via a hybrid superwettable coating with superhydrophobic and superhydrophilic nanoparticles. Appl Surf Sci 2019;465:986–94. https://doi.org/10.1016/j.apsusc.2018.09.210.
[27] Kasanen J, Suvanto M, Pakkanen TT. Self-cleaning, titanium dioxide based, multilayer coating fabricated on polymer and glass surfaces. J Appl Polym Sci 2009;111(5):2597–606. https://doi.org/10.1002/app.29295.
[28] Banerjee S, Dionysiou DD, Pillai SC. Self-cleaning applications of TiO2 by photo-induced hydrophilicity and photocatalysis. Appl Catal B Environ 2015;176:396–428. https://doi.org/10.1016/j.apcatb.2015.03.058.
[29] Sobczyk-Guzenda A, Gazicki-Lipman M, Szymanowski H, Kowalski J, Wojciechowski P, Halamus T. Characterization of thin TiO2 films prepared by plasma enhanced chemical vapour deposition for optical and photocatalytic applications. Thin Solid Films 2009;517(18):5409–14. https://doi.org/10.1016/j.tsf.2009.01.010.
[30] Luo Q, Cai Q, Li X, Chen X. Characterization and photocatalytic activity of large-area single crystalline anatase TiO2 nanotube films hydrothermal synthesized on Plasma electrolytic oxidation seed layers. J Alloys Compd 2014;597:101–9. https://doi.org/10.1016/j.jallcom.2014.01.216.
[31] Shavdina O, Berthod L, Kämpfe T, Reynaud S, Veillas C, Verrier I, et al. Large area fabrication of periodic TiO2 nanopillars using microsphere photolithography on a photopatternable sol-gel film. Langmuir 2015;31(28):7877–84. https://doi.org/10.1021/acs.langmuir.5b01191.
[32] Ghannadi S, Abdizadeh H, Golobostanfard MR. Modelling the current density in sol–gel electrophoretic deposition of titania thin film. Ceram Int 2014;40:2121–6. https://doi.org/10.1016/j.ceramint.2013.07.128.
[33] Mohite VS, Mahadik MA, Kumbhar SS, Kothavale VP, Moholkar AV, Rajpure KY, et al. Photoelectrocatalytic degradation of benzoic acid using sprayed TiO2 thin films. Ceram Int 2015;41:2202–8. https://doi.org/10.1016/j.ceramint.2014.10.020.

[34] Zhu X, Gu P, Wu H, Yang D, Sun H, Wangyang P, et al. Influence of substrate on structural, morphological and optical properties of TiO2 thin films deposited by reaction magnetron sputtering. AIP Adv 2017;7:125326. https://aip.scitation.org/doi/full/10.1063/1.5017242.
[35] Fontana LC, Muzart JLR. Triode magnetron sputtering TiN film deposition. Surf Coating Technol 1999;114:7–12. https://doi.org/10.1016/S0257-8972(99)00032-8.
[36] Stryhalski J. Propriedades óticas e elétricas de filmes de óxido de titânio dopados com nióbio. Universidade do Estado de Santa Catarina - UDESC (Tese de Doutoramento); 2015.
[37] Miao L, Tanemura S, Watanabe H, Mori Y, Kaneko K, Toh S. The improvement of optical reactivity for TiO2 thin films by N2–H2 plasma surface-treatment. J Cryst Growth 2004;260(1–2):118–24. https://doi.org/10.1016/j.jcrysgro.2003.08.010.
[38] Philippsen ME, Tomiyama M, do Rosario Irala D, Stryhalski J, Fontana LC. Molhabilidade de filmes de TiO2 Depositados sobre substratos de vidro soda-lime. Revista Brasileira de Aplicações de Vácuo 2017;35(3):128–32. https://doi.org/10.17563/rbav.v35i3.1029.
[39] Mohamed SH, Alhazime Ali A. Suppressing photoluminescence and enhancing light absorption of TiO2 via using TiO2/TiN/TiO2 plasmonic multilayers for better solar harvesting. J Mater Res Technol 2022;18:4470–8. https://doi.org/10.1016/j.jmrt.2022.04.132.
[40] Li F, Li Q, Kim H. Spray deposition of electrospun TiO2 nanoparticles with self-cleaning and transparent properties onto glass. Appl Surf Sci 2013;276:390. https://doi.org/10.1016/j.apsusc.2013.03.103.
[41] Fox M. Optical properties of solids. Oxford: Oxford University Press; 2001. -13: 978-0199573370.
[42] Wang YH, Rahman KH, Wu CC, Chen KC. A Review on the pathways of the improved structural characteristics and photocatalytic performance of Titanium Dioxide (TiO2) thin films fabricated by the magnetron-sputtering technique. Catalysts 2020;10:598. https://doi.org/10.3390/catal10060598.
[43] Lindgren T, Mwabora JM, Avendano E, Jonsson J, Hoel A, Granqvist CG, et al. Photoelectrochemical and optical properties of nitrogen doped titanium dioxide films prepared by reactive DC magnetron sputtering. J Phys Chem B 2003;107:5709–16. https://doi.org/10.1021/jp027345j.
[44] Sun Y, Sun S, Liao X, Wen J, Yin G, Pu X. Effect of heat treatment on surface hydrophilicity-retaining ability of titanium dioxide nanotubes. Appl Surf Sci 2018;440:440–7. https://doi.org/10.1016/j.apsusc.2018.01.136.
[45] Tauc J, Grigorovici R, Vancu A. Optical properties and electronic structure of amorphous germanium. Phys Status Solidi 1966;15:627–37. https://doi.org/10.1002/pssb.19660150224.
[46] Han M, Jiang K, Zhang J, Yu W, Li Y, Hu Z, et al. Structural, electronic band transition and optoelectronic properties of delafossite CuGa1-xCrxO2 ($0 \leq x \leq 1$) solid solution films grown by the sol–gel method. J Mater Chem 2012;22:18463–70. https://doi.org/10.1039/c2jm33027j.
[47] Vieira TM, Sagás JC, Pessoa RS, Fontana LC. Multiphase titanium suboxides films grown on glass substrate: surface energy, wettability and morphology analysis. Surface Interfac 2020;20:100610. https://doi.org/10.1016/j.surfin.2020.100610. ISSN 2468-0230.
[48] Serio S, Jorge MM, Nunes Y, Barradas NP, Alves E, Munnik F. Incorporation of N in TiO2 films grown by DC-reactive magnetron sputtering, Nucl Instrum Methods. Phys. Res. Sec. B 2012;273:109–12. https://doi.org/10.1016/j.nimb.2011.07.052.
[49] Aubry E, Ghazzal MN, Demange V, Chaoui N, Robert D, Billard A. Surf Coating Technol 25 June 2007;201(18):7706–12. https://doi.org/10.1016/j.surfcoat.2007.03.003.
[50] Naz MY, Shukrullah S, Rehman SU, Khan Y, Al-Arainy AA, Meer R. Optical characterization of non-thermal plasma jet energy carriers for effective catalytic processing of industrial wastewaters. Sci Rep 2021;11(1):1–13. https://doi.org/10.1038/s41598-021-82019-4.
[51] Dubey RS. Temperature-dependent phase transformation of TiO2 nanoparticles synthesized by sol–gel method. Mater Lett 2018;215:312–7. https://doi.org/10.1016/j.matlet.2017.12.120.
[52] Chang SC, Li TH, Chan HT. Hydrogen plasma annealed titanium dioxide oxide/aluminum-doped zinc oxide films applied in low emissivity glass. Int J Electrochem Sci 2021;16:8. https://doi.org/10.3390/ma15093292.
[53] Panicaud B, Grosseau-Poussard JL, Girault P, Dinhut JF, Thiaudiere D. Comparison of growth stress measurements with modelling in thin iron oxide films. Appl Surf Sci 2006;252(24):8414–20. https://doi.org/10.1016/j.apsusc.2005.07.075.
[54] Fujishima A, Rao TN, Tryk DA. Titanium dioxide photocatalysis. Photochem Photobiol C 2000;1:1–21. https://doi.org/10.1016/S1389-5567(00)00002-2.
[55] Hossain MN, Lee SJ, Kim CL. Fabrication of TiO2–KH550–PEG super-hydrophilic coating on glass surface without UV/plasma treatment for self-cleaning and anti-fogging applications. Materials 2022;15(9):3292. https://doi.org/10.3390/ma15093292.
[56] Wang X, Ding H, Lv G, Zhou R, Ma R, Hou X, et al. Fabrication of superhydrophilic self-cleaning SiO2–TiO2 coating and its photocatalytic performance. Ceram Int 2022;48(14):20033–40. https://doi.org/10.1016/j.ceramint.2022.03.278.
[57] Syafiq A, Balakrishnan V, Rahim NA. Durable self-cleaning nano-titanium dioxide superhydrophilic coating with anti-fog property. Pigm Resin Technol 2022. ahead-of-print. ISSN: 0369-9420.